

# Cu-Supported ZnO under Conditions of CO<sub>2</sub> Reduction to Methanol: Why 0.2 ML Coverage?

Robert H. Lavroff,<sup>▽</sup> Edison Cummings,<sup>▽</sup> Kaustubh Sawant, Zisheng Zhang, Philippe Sautet,<sup>\*</sup> and Anastassia N. Alexandrova<sup>\*</sup>



Cite This: *J. Phys. Chem. Lett.* 2024, 15, 11745–11752



Read Online

ACCESS |



Metrics & More



Article Recommendations



Supporting Information

**ABSTRACT:** By hydrogenating carbon dioxide to value-added products such as methanol, heterogeneous catalysts can lower greenhouse gas emissions and generate alternative liquid fuels. The most common commercial catalyst for the reduction of CO<sub>2</sub> to methanol is Cu/ZnO/Al<sub>2</sub>O<sub>3</sub>, where ZnO improves conversion and selectivity toward methanol. The structure of this catalyst is thought to be Zn oxy(hydroxyl) overlayers on the nanometer scale on Cu. In the presence of CO<sub>2</sub> and H<sub>2</sub> under reaction conditions, the Cu substrate itself can be restructured and/or partially oxidized at its interface with ZnO, or the Zn might be reduced, possibly completely to a CuZn alloy, making the exact structure and stoichiometry of the active site a topic of active debate. In this study, we examine Zn<sub>3</sub> clusters on Cu(100) and Cu(111), as a subnano model of the catalyst. We use a grand canonical genetic algorithm to sample the system structure and stoichiometry under catalytic conditions: *T* of 550 K, initial partial pressures of H<sub>2</sub> of 4.5 atm and CO<sub>2</sub> of 0.5 atm, and 1% conversion. We uncover a strong dependence of the catalyst stoichiometry on the surface coverage. At the optimal 0.2 ML surface coverage, chains of Zn(OH) form on both Cu surfaces. On Cu(100), the catalyst has many thermally accessible metastable minima, whereas on Cu(111), it does not. No oxidation or reconstruction of the Cu is found. However, at a lower coverage of Zn, Zn<sub>3</sub> clusters take on a metallic form on Cu(100), and slightly oxidized Zn<sub>3</sub>O on Cu(111), while the surface uptakes H to form a variety of low hydrides of Cu. We thus hypothesize that the 0.2 ML Zn coverage is optimal, as found experimentally, because of the stronger yet incomplete oxidation afforded by Zn at this coverage.



Heterogeneous catalysis is essential to chemical production, sustainable energy, and many other important aspects of society, but it remains a difficult science to study experimentally and computationally because catalysts, particularly their active sites, can be rebuilt drastically at each step of the reaction. The dynamic nature of these catalysts under reaction conditions leaves many outstanding questions in the field.<sup>1–6</sup> One contested question is the true nature of the active site in various heterogeneous catalytic reactions, and here we will focus on the reduction of CO<sub>2</sub> to methanol on Cu/Zn/ZnO catalysts.<sup>7–12</sup> In this industrial reaction, CO<sub>2</sub> and H<sub>2</sub> gases flowed over the catalyst and are believed to pass through formate and methoxide intermediates before ultimately forming methanol.<sup>13</sup> Because oxidation, reduction, and associated restructuring of the Cu–Zn interface can occur under reaction conditions, this system is a key example of strong metal support interaction (SMSI) and has led to various computational and experimental studies proposing different active sites with little consensus,<sup>14–16</sup> though Zn in some oxidation state being encapsulated on Cu as an overlayer is accepted as a key step for the Cu/ZnO/Al<sub>2</sub>O<sub>3</sub> industrial catalyst.<sup>16,17</sup> Oxide-on-metal “inverse catalysts” have also been shown to perform better than their traditional, metal-on-oxide counterparts for a number of reactions,<sup>18–28</sup> including

methanol synthesis with ZnO or ceria on copper.<sup>29,30</sup> Across these many variants, catalytic Zn has been proposed to be metallic (as an alloy)<sup>8,10,15,31–33</sup> or to exist in small ZnO surface islands,<sup>30,34–37</sup> bulk/layered forms of ZnO,<sup>17</sup> or a mixed phase of all of these.<sup>38–41</sup> The copper coordination and oxidation state is also contested.<sup>33,39,42–44</sup> It has also been proposed that Zn coverage is highly dynamic, responding to the chemical potential of the surrounding gases.<sup>10,33,42</sup>

Clearly, a reliable phase diagram of this catalyst would be helpful in understanding its active site, and though one has been presented, it considered only oxygen chemical potentials and not hydrogen;<sup>34</sup> on the contrary, hydrogen is present in methanol hydrogenation and known to be a major factor in ZnO thin film restructuring on metals.<sup>45</sup> One consensus that has largely been reached is that this methanol reduction catalyst is most efficient at a 20% surface coverage of Zn on Cu

**Received:** October 7, 2024

**Revised:** November 9, 2024

**Accepted:** November 12, 2024

**Published:** November 15, 2024



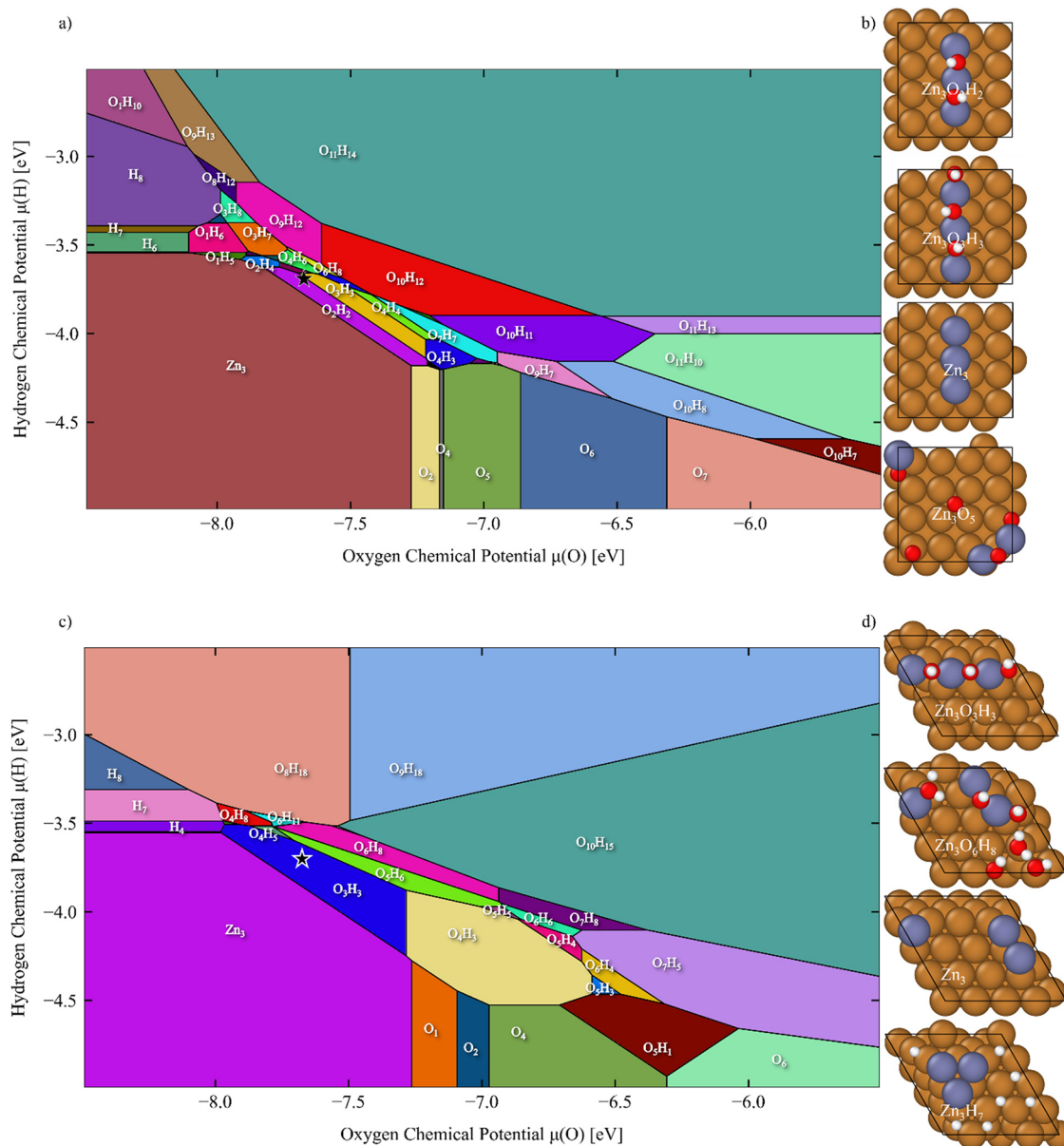


**Figure 1.** Phase diagrams of (a)  $\text{Zn}_3/\text{Cu}(100)$  and (c)  $\text{Zn}_3/\text{Cu}(111)$  at 0.2 ML coverage as a function of the chemical potentials of O and H. The black star denotes the chemical potentials for the considered reaction conditions. The dominant structures of several phases are shown in panel b for  $\text{Zn}_3/\text{Cu}(100)$  and panel d for  $\text{Zn}_3/\text{Cu}(111)$  as top-down views.

(0.2 ML).<sup>7,32,46–48</sup> This begs the question of why 0.2 ML is optimal.

Given this information, we constructed a computational model in which a small Zn cluster is deposited on a Cu unit cell to match the 0.2 ML coverage. Here, we select  $p(4 \times 4)$  Cu surface supercells with (111) and (100) termination, because model catalysts made by deposition of ZnO on these two single crystal surfaces were shown to be highly active, with (100) reported to be superior to (111).<sup>48</sup> We perform the grand canonical global optimization under a variety of chemical potentials of hydrogen and oxygen to obtain a phase diagram as a function of these chemical potentials. By determining the chemical potentials of the reaction conditions using ab initio thermodynamics, we arrive at the most stable phases corresponding to those conditions. By comparing the results to those at a smaller Zn coverage on Cu ( $\sim 0.14$  ML), we find a strong dependence of the system stoichiometry (O and H

content) on the Zn coverage, potentially shedding light on why 0.2 ML appears to be optimal in the experiment.

The chemical potentials are derived on the basis of the conditions of the thermal  $\text{CO}_2$  reduction of Palomino et al.:<sup>48</sup>  $T$  of 550 K, initial partial pressure of  $\text{H}_2$  of 4.5 atm, and initial partial pressure of  $\text{CO}_2$  of 0.5 atm. Assuming 1% conversion to match the experiments of Palomino et al.,<sup>48</sup> we obtain reaction partial pressures of 0.005 atm for  $\text{H}_2\text{O}$  and  $4.5 - 3(0.005) = 4.485$  atm for  $\text{H}_2$ . We compute the free energies ( $G$ ) of  $\text{H}_2\text{O}$  and  $\text{H}_2$  using the density functional theory (DFT) energies plus zero-point energy (ZPE) as the enthalpy ( $H$ ) and the ideal gas limit of the vibrational, translational, and rotational entropy ( $S$ ) contributions:

$$G(T, P) = H(T) - TS(T, P) = E_{\text{DFT}} + E_{\text{ZPE}} - T(S_{\text{trans}} + S_{\text{vib}} + S_{\text{rot}})$$

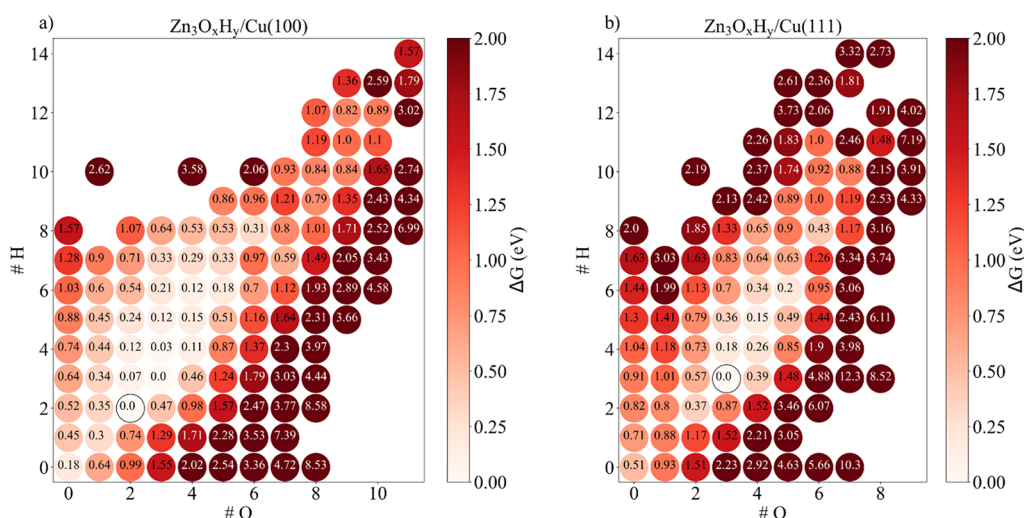


**Figure 2.** Free energy surfaces as functions of O and H coverage for (a) Cu(100) and (b) Cu(111), at 0.2 ML coverage, using the following chemical potentials:  $\mu_{\text{O}} = 7.677$  eV and  $\mu_{\text{H}} = 3.685$  eV. Darker reds indicate higher free energies, which are relative to each surface's GM (i.e.,  $\Delta G_{\text{GM}} = 0.0$  eV). The plots are based on the global minimum free energy structure of each stoichiometry.

Using the fact that free energy is gained when a molecule adsorbs to the Cu/Zn surface, we obtain chemical potentials of  $\mu(\text{H}) = \mu(\text{H}_2)/2 = -3.684$  eV per H and  $\mu(\text{O}) = \mu(\text{H}_2\text{O}) - \mu(\text{H}_2) = -8.107$  eV per O.

Thus far, however, this derivation has assumed that the free energy of formation of ZnO is zero or negligible, which it is not. The ZnO formation equilibrium will give a more positive surface oxygen chemical potential:

$$\mu(\text{O}) = \mu(\text{H}_2\text{O}) - \mu(\text{H}_2) - \Delta G_{\text{f}}(\text{ZnO}, 0 \text{ K})$$

where

$$\begin{aligned} \Delta G_{\text{f}}(\text{ZnO}, 0 \text{ K}) &= E_{\text{DFT}}(\text{ZnO}) + E_{\text{ZPE}}(\text{ZnO}) \\ &- [E_{\text{DFT}}(\text{Zn}) + E_{\text{ZPE}}(\text{Zn}) + \frac{1}{2}E_{\text{DFT}}(\text{O}_2) + \frac{1}{2}E_{\text{ZPE}}(\text{O}_2)] \end{aligned}$$

Because the PBE exchange-correlation functional used in this study notoriously overestimates the bond energy of O<sub>2</sub>, for  $\Delta G_{\text{f}}(\text{ZnO}, 0 \text{ K})$ , we employ optPBE exchange<sup>49</sup> instead of PBE exchange (but keep PBE correlation) to evaluate the free energy of formation of ZnO, maintaining the use of a very similar GGA-family density functional for the sake of consistency, but mitigating the error associated with O<sub>2</sub>. As a result,  $\mu(\text{O})$  is shifted by 0.43 eV to  $-7.677$  eV per O. For comparison, using PBE exchange instead of optPBE gives a shift of 0.39 eV; the difference is small but not negligible due to the many domains present near reaction conditions on Cu(100) shown below.

Grand canonical global optimization using GCGA (see Methods for details) was performed at several chemical potentials of O and H, where global and local minima were retained. For intermediate values of the chemical potentials, the free energies of all found isomers were re-evaluated, and thus, the phase diagram was made continuous by extrapolation. The resultant phase diagrams of Zn<sub>3</sub>/Cu(100) and Zn<sub>3</sub>/Cu(111) as a function of  $\mu(\text{O})$  and  $\mu(\text{H})$  are presented in Figure 1. The black star denotes the chemical potentials under the specific considered reaction conditions, derived in the previous section. Different visualizations of these phases, such as individual diagrams for H coverage and O coverage, are available in Figure S1 for Cu(100) and Figure S2 for Cu(111).

A clear difference between Cu(100) (Figure 1a) and Cu(111) (Figure 1c) is that Cu(100) has much narrower domains that can interconvert at even small changes to the chemical potential, particularly at and around reaction conditions. This suggests an ease of changing the oxidation and hydroxylation status of Zn, which is relevant to the reactivity. By contrast, the domains tend to be wider in the Cu(111) diagram, indicating greater ranges of stability, consistent with the Cu(100) surface being known to be more reactive, while Cu(111) is more stable.

Upon close examination of only the reaction chemical potentials, calculated free energy surfaces as functions of the number of O and H atoms are shown in Figure 2. On the Cu(100) and Cu(111) surfaces, the catalysts have clear free energy basins, with the minimum free energy (designated as 0.0 eV) corresponding to Zn<sub>3</sub>O<sub>2</sub>H<sub>2</sub> and Zn<sub>3</sub>O<sub>3</sub>H<sub>3</sub> for Cu(100) (Figure 2a) and to Zn<sub>3</sub>O<sub>3</sub>H<sub>3</sub> for Cu(111) (Figure 2b). The value of  $k_{\text{B}}T$  at 550 K is  $\sim 0.0474$  eV, making the Zn<sub>3</sub>O<sub>3</sub>H<sub>4</sub> local minimum (LM) structures easily thermally accessible on Cu(100). A deeper basin exists around the global minimum (GM) on Cu(111), however, leading to lower probabilities of other stoichiometries being thermally accessed. This corresponds to the most likely resting states of the catalyst and may change when reaction intermediates are adsorbed to the catalyst (to be addressed in a future study). Structures with many hydrogen atoms and few oxygen atoms or vice versa are either highly unfavorable or absent altogether under these conditions, especially in the case of many oxygens but few hydrogens. This indicates the favorability of hydroxyl and (less so) water ligands, which is verified in the next section where GM and LM structures are discussed. The stoichiometric or near-stoichiometric oxide or metallic forms of the cluster are clearly not identified as being relevant.

At 0.2 ML coverage, the lowest-lying minima are very similar chain-like structures, often differing by small Zn–Zn bond angles and by additions of chemisorbed water molecules, which are essentially guaranteed to overcome the desorption barrier at 550 K, leaving only hydroxyls. This is true even upon comparison of (100) and (111) surfaces, though two notable differences are that energy differences on Cu(100) are quite small between varying hydroxyl and hydride content, and a

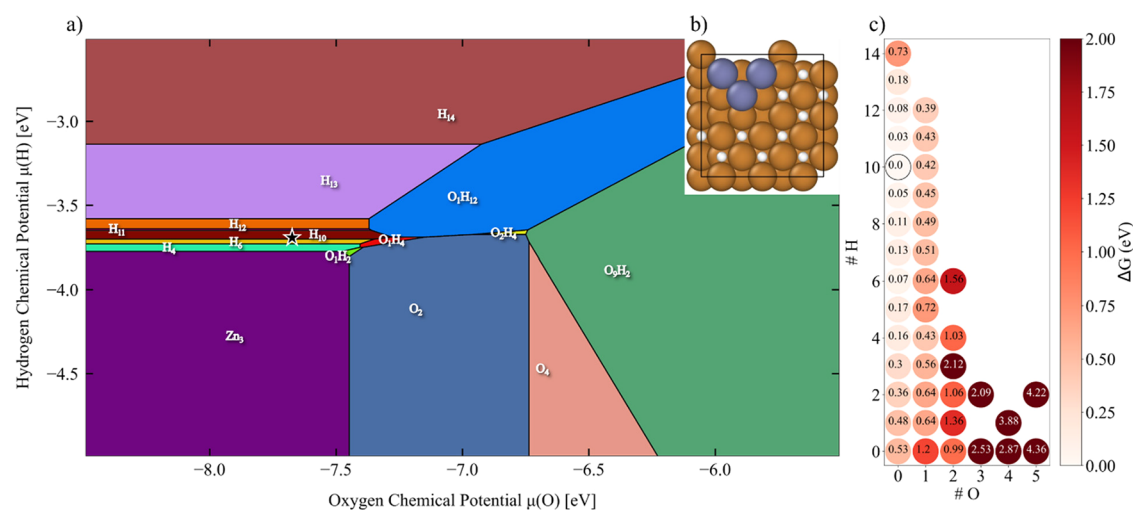


**Figure 3.** (a) Phase diagram, (b) global minimum structure of  $Zn_3O_xH_y$  on Cu(100), and (c) free energy surface at a 0.14 ML coverage. Note that all LMs differ from the GM only by copper surface hydride coverage.

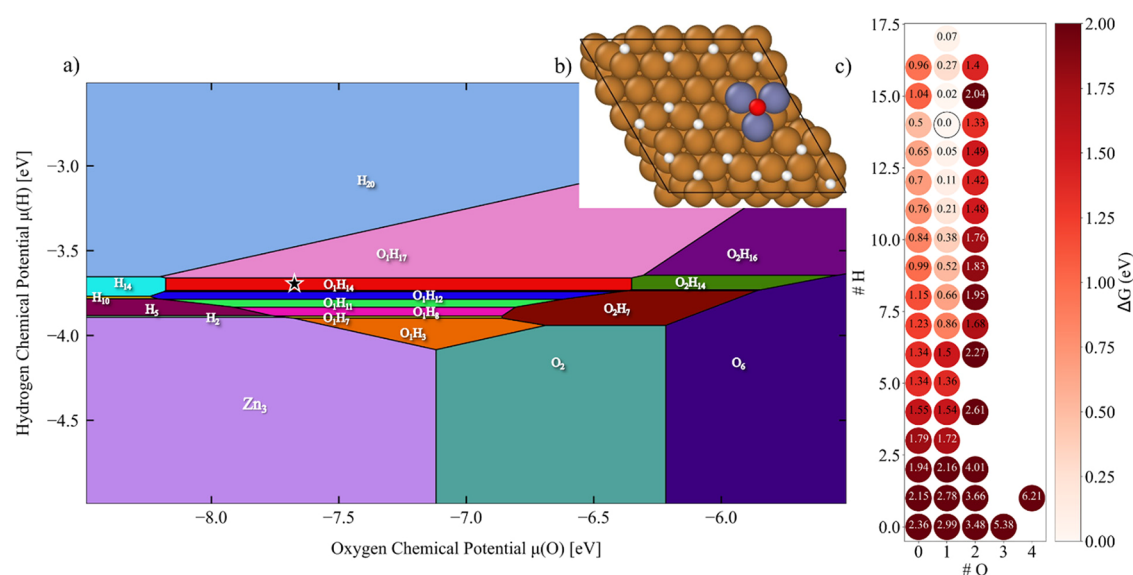


**Figure 4.** (a) Phase diagram, (b) global minimum structure of  $Zn_3O_xH_y$  on Cu(111), and (c) free energy surface at a 0.14 ML coverage. Note that all LMs differ from the GM only by copper surface hydride coverage.

ring-like structure (Figure S7, LM3) is also quite stable on Cu(100). This is consistent with the depth of the wells in the free energy surfaces (Figure 2a) and implies that the true industrial catalyst may be fluxional in its (100) regions and restructure significantly when different intermediates bind to it.<sup>50</sup>

Notably,  $Zn_3(OH)_3$  chains bridge periodic images in Figure S9 LM1 (also shown Figure 1b), and the structure is essentially degenerate in free energy with the GM, at a difference of only 0.004 eV, which is well within the margin of error for not only DFT but also more accurate electronic structure methods. The GM on the Cu(111) also shows the bonding of Zn to its image under the periodic boundary conditions of the unit cell, indicating that long chains of  $Zn(OH)$  would form if larger, more physical supercells were used and the 0.2 ML coverage was kept fixed.<sup>51,52</sup> Due to the sites bridging Cu, which the Zn atoms favor on both surfaces, being spaced more closely on Cu(100), such chains form; it would take a fourth Zn atom for the same chains to form on the (100) facet as a GM on (111).

Notably, while we show below that O and H coverages are highly sensitive to reaction conditions, Li et al. found a very similar (though not bridging periodic images), chain-like minimum structure on  $p(6 \times 6)$  Cu(111) slabs under conditions of methanol steam reforming, a reaction at a similar temperature but with very different amounts of O and H present.<sup>53</sup>

Hence, at the 0.2 ML coverage, the  $Zn_3(OH)_3$  chains interacting with their periodic images lead to an increase in the extents of favorable bond formation. This is not an artifact, as the coverage emulates the experimentally synthesized catalyst, but it does beg the question of how the  $Zn_3$  would behave if the Cu slab were too large to form these cell-bridging chains, or in other words if the coverage of Zn was  $<0.2$  ML. We thus perform sampling of the same 3Zn system but on  $6 \times 6$  slabs with (100) and (111) termination, corresponding to a 0.14 ML Zn coverage, and found drastically different behavior, shown in Figures 3 and 4. The  $Zn_3$  clusters are no longer hydroxylated. The GM and LMs on Cu(100) are bare  $Zn_3$  in a

triangular formation, and the same is true on Cu(111) except with an oxygen atom bridging them as predicted by Reichenbach et al.<sup>34</sup> Hydrogen adsorbs to the Cu surface rather than the Zn, at a significant coverage. This result, obtained under conditions of CO<sub>2</sub> reduction, is in stark contrast to the previously mentioned case of methanol steam reforming studied by Li et al.<sup>53</sup> We also note the lack of many metastable Zn<sub>3</sub> geometries on Cu(111).

Finally, we note that brass, a mixture of Cu and Zn, is among the most famous alloys in existence. It is thus natural to wonder whether surface alloying may occur between the Zn<sub>3</sub> cluster and Cu under the reaction conditions. During all sampling simulations presented above, the surface Cu atoms were sampled and, in particular, allowed to swap places with Zn; no alloyed phases were identified. To confirm the result, the low-free energy structures on Cu(100) and Cu(111), such as the Zn(OH) chains, were altered with this swapping by hand, to see if additional minima were discovered. While surface alloy structures were favorable at more negative oxygen chemical potentials [i.e.,  $\mu(\text{O}) = -8.1$  eV], none were found to be accessible minima under reaction conditions. Thus, alloys can be ruled out as the active phase, at least at the level of a small model.

In the important catalytic reaction of thermal CO<sub>2</sub> reduction to methanol via zinc/zinc oxide on copper, the true nature of the active site under reaction conditions has been widely contested. Using the Zn<sub>3</sub> cluster on p(4 × 4) supercells of Cu(100) and Cu(111) to represent the optimal 0.2 ML coverage for this reaction, we present a comprehensive phase diagram of hydrogen and oxygen coverage as a function of their respective chemical potentials. We find that the more reactive facet, Cu(100), has many energetically similar surface phases near the reaction chemical potentials, while the more stable facet, Cu(111), is more sparse in its phases. For both, we predict that chains of zinc-hydroxyl spanning the copper surface are the global minima, with some variation of hydroxyl content, geometry, and surface hydrides easily thermally accessible for Zn<sub>3</sub>/Cu(100) but not Zn<sub>3</sub>/Cu(111). The fully oxidized Zn<sub>3</sub>O<sub>3</sub> phase is not competitive, and Cu/Zn surface alloying is also not observed under the reaction conditions. We observe an important dependence of the preferred structures and stoichiometries of Zn on the coverage. The previously experimentally identified 0.2 ML coverage is a critical coverage at which chains of Zn hydroxide can reach across the unit cell boundary, forming extended structures generally supported by the increased number of Zn–O bonds. These extended structures are apparently required for Zn to be partially oxidized. At lower coverages, e.g., 0.14 ML, simulations show isolated metallic or very mildly oxidized Zn clusters and larger amounts of surface hydride on Cu. This drastic change may point at the reason for the optimal coverage to be in the experimentally determined range of 0.2 ML, because on the contrary, a higher coverage could lead to blocking of surface active sites. The structures found establish important starting points for reactivity studies of industrial reduction of CO<sub>2</sub> to methanol.

## METHODS

All calculations were performed with periodic DFT, using the Vienna Ab-Initio Software Package (VASP).<sup>54–56</sup> The Perdew–Burke–Ernzerhof (PBE)<sup>57</sup> functional (known to perform well for the surface and bulk properties of transition metals)<sup>58</sup> was used with corresponding pseudopotentials in the

projector-augmented wave (PAW) scheme,<sup>59</sup> with a plane wave kinetic energy cutoff of 400 eV. The zero-damping DFT-D3 method<sup>60</sup> was used to account for van der Waals corrections, and a dipole correction<sup>61</sup> in the Z-direction was applied. The self-consistency for energy was enforced up to 10<sup>−5</sup> eV and for force norms up to 0.06 eV/Å in geometry optimizations. Due to the highly ionic bonding of Zn and O, no Hubbard corrections (*U* or *V*) or Hund corrections (*J*) were used. Energy differences between low-lying gas phase isomers were computed with *U* and *J* combinations ranging from 0 to 5 eV each, in increments of 0.5 eV, and compared against the HSE06<sup>62</sup> range-separated hybrid functional, and indeed, calculations with no Hubbard terms were found to match the HSE06 results most closely. To mimic the desired 0.2 ML coverage of ZnO, a p(4 × 4) Cu supercell was used with four layers for the Cu(100) and Cu(111) surfaces. The top two of these layers were unconstrained during the optimization to allow for any surface deformation. A 20 Å vacuum was used to avoid interaction between slabs. A  $\Gamma$ -only *k*-point scheme was applied, justified by the large size of the supercell (the area of the (100) surface is ~100 Å<sup>2</sup>, for example). Second-order Methfessel–Paxton smearing was used to assist convergence, but all energies were taken in the limit of zero smearing. Manual sampling of structures on Cu surfaces, as well as ab initio thermochemistry calculations (i.e., ideal gas entropic contributions) for determining chemical potentials, was performed with the atomic simulation environment (ASE).<sup>63,64</sup> Grand canonical genetic algorithm (GCGA) global optimization was performed using our group's in-house GOCIA software.<sup>65</sup> Fifty initial structures were generated randomly and optimized with the energy and force cutoffs given above, with manual prevention of forming H–H or O–O bonds. All structure visualization was performed with Ovito.<sup>66</sup>

## ASSOCIATED CONTENT

### Supporting Information

The Supporting Information is available free of charge at <https://pubs.acs.org/doi/10.1021/acs.jpcllett.4c02908>.

Auxiliary phase diagrams and structures relative to chemical potential (PDF)

## AUTHOR INFORMATION

### Corresponding Authors

**Philippe Sautet** – Department of Chemistry and Biochemistry, Department of Chemical and Biomolecular Engineering, and California NanoSystems Institute, University of California, Los Angeles, Los Angeles, California 90095-1569, United States; [orcid.org/0000-0002-8444-3348](https://orcid.org/0000-0002-8444-3348); Email: [sautet@ucla.edu](mailto:sautet@ucla.edu)

**Anastassia N. Alexandrova** – Department of Chemistry and Biochemistry, Department of Materials Science and Engineering, and California NanoSystems Institute, University of California, Los Angeles, Los Angeles, California 90095-1569, United States; [orcid.org/0000-0002-3003-1911](https://orcid.org/0000-0002-3003-1911); Email: [ana@chem.ucla.edu](mailto:ana@chem.ucla.edu)

### Authors

**Robert H. Lavroff** – Department of Chemistry and Biochemistry, University of California, Los Angeles, Los Angeles, California 90095-1569, United States; [orcid.org/0000-0002-6133-5766](https://orcid.org/0000-0002-6133-5766)

Edison Cummings – Department of Chemistry and Biochemistry, University of California, Los Angeles, Los Angeles, California 90095-1569, United States

Kaustubh Sawant – Department of Chemical and Biomolecular Engineering, University of California, Los Angeles, Los Angeles, California 90095-1569, United States

Zisheng Zhang – Department of Chemistry and Biochemistry, University of California, Los Angeles, Los Angeles, California 90095-1569, United States; [orcid.org/0000-0002-4370-4038](https://orcid.org/0000-0002-4370-4038)

Complete contact information is available at:  
<https://pubs.acs.org/10.1021/acs.jpcllett.4c02908>

### Author Contributions

<sup>†</sup>R.H.L. and E.C. contributed equally to this work.

### Notes

The authors declare no competing financial interest.

## ACKNOWLEDGMENTS

P.S. and A.N.A. acknowledge U.S. Department of Energy (DOE) BES Grant DE-SC0019152. R.H.L. and E.C. performed the calculations on the DOE National Energy Research Scientific Computing Center (NERSC) supercomputers under Contract DE-AC02-05CH11231. R.H.L. acknowledges support by the National Science Foundation Graduate Research Fellowship under Grant DGE-2034835. An additional award of computer time was provided by the Innovative and Novel Computational Impact on Theory and Experiment (INCITE) program. This research used resources of the Argonne Leadership Computing Facility, which is a DOE Office of Science User Facility supported under Contract DE-AC02-06CH11357.

## REFERENCES

- (1) Kalz, K. F.; Kraehnert, R.; Dvoyashkin, M.; Dittmeyer, R.; Gläser, R.; Krewer, U.; Reuter, K.; Grunwaldt, J. D. Future Challenges in Heterogeneous Catalysis: Understanding Catalysts under Dynamic Reaction Conditions. *ChemCatChem* **2017**, *9* (1), 17–29.
- (2) Zhang, Z.; Zandkarimi, B.; Alexandrova, A. N. Ensembles of Metastable States Govern Heterogeneous Catalysis on Dynamic Interfaces. *Acc. Chem. Res.* **2020**, *53* (2), 447–458.
- (3) Lavroff, R. H.; Morgan, H. W. T.; Zhang, Z.; Poets, P.; Alexandrova, A. N. Ensemble Representation of Catalytic Interfaces: Soloists, Orchestras, and Everything in-Between. *Chem. Sci.* **2022**, *13* (27), 8003–8016.
- (4) Satterfield, C. N. *Heterogeneous Catalysis in Industrial Practice*, 2nd ed.; 1991.
- (5) Somorjai, G. A.; Mujumdar, A. S. Introduction to Surface Chemistry and Catalysis. *Drying Technol.* **1995**, *13* (1–2), 507–508.
- (6) Nørskov, J. K.; Studt, F.; Abild-Pedersen, F.; Bligaard, T. *Fundamental Concepts in Heterogeneous Catalysis*; 2014; Vol. 9781118888957.
- (7) Kattel, S.; Ramirez, P. J.; Chen, J. G.; Rodriguez, J. A.; Liu, P. Active Sites for CO<sub>2</sub> Hydrogenation to Methanol on Cu/ZnO Catalysts. *Science* **2017**, *355* (6331), 1296–1299.
- (8) Nakamura, J.; Fujitani, T.; Kuld, S.; Helveg, S.; Chorkendorff, I.; Sehested, J. Comment on “Active Sites for CO<sub>2</sub> Hydrogenation to Methanol on Cu/ZnO Catalysts. *Science* **2017**, *357* (6354), aan8074 DOI: [10.1126/science.aan8074](https://doi.org/10.1126/science.aan8074).
- (9) Kattel, S.; Ramirez, P. J.; Chen, J. G.; Rodriguez, J. A.; Liu, P. Response to Comment on “Active Sites for CO<sub>2</sub> Hydrogenation to Methanol on Cu/ZnO Catalysts. *Science* **2017**, *357* (6354), aan8210 DOI: [10.1126/science.aan8210](https://doi.org/10.1126/science.aan8210).
- (10) Behrens, M.; Studt, F.; Kasatkin, I.; Kühl, S.; Hävecker, M.; Abild-Pedersen, F.; Zander, S.; Girsig, F.; Kurr, P.; Knief, B. L.; Tovar, M.; Fischer, R. W.; Nørskov, J. K.; Schlögl, R. The Active Site of Methanol Synthesis over Cu/ZnO/Al<sub>2</sub>O<sub>3</sub> Industrial Catalysts. *Science* **2012**, *336* (6083), 893–897.
- (11) Laudenschlager, D.; Ruland, H.; Muhler, M. Identifying the Nature of the Active Sites in Methanol Synthesis over Cu/ZnO/Al<sub>2</sub>O<sub>3</sub> Catalysts. *Nat. Commun.* **2020**, *11* (1), 3898 DOI: [10.1038/s41467-020-17631-5](https://doi.org/10.1038/s41467-020-17631-5).
- (12) Choi, Y.; Futagami, K.; Fujitani, T.; Nakamura, J. The Difference in the Active Sites for CO<sub>2</sub> and CO Hydrogenations on Cu/ZnO-Based Methanol Synthesis Catalysts. *Catal. Lett.* **2001**, *73* (1), 27.
- (13) Guil-López, R.; Mota, N.; Llorente, J.; Millán, E.; Pawelec, B.; Fierro, J. L. G.; Navarro, R. M. Methanol Synthesis from CO<sub>2</sub>: A Review of the Latest Developments in Heterogeneous Catalysis. *Materials* **2019**, *12* (23), 3902.
- (14) Holse, C.; Elkjær, C. F.; Nierhoff, A.; Sehested, J.; Chorkendorff, I.; Helveg, S.; Nielsen, J. H. Dynamic Behavior of CuZn Nanoparticles under Oxidizing and Reducing Conditions. *J. Phys. Chem. C* **2015**, *119* (5), 2804–2812.
- (15) Kuld, S.; Conradsen, C.; Moses, P. G.; Chorkendorff, I.; Sehested, J. Quantification of Zinc Atoms in a Surface Alloy on Copper in an Industrial-Type Methanol Synthesis Catalyst. *Angew. Chem., Int. Ed.* **2014**, *53* (23), 5941–5945.
- (16) Schott, V.; Oberhofer, H.; Birkner, A.; Xu, M.; Wang, Y.; Muhler, M.; Reuter, K.; Wöll, C. Chemical Activity of Thin Oxide Layers: Strong Interactions with the Support Yield a New Thin-Film Phase of ZnO. *Angew. Chem., Int. Ed.* **2013**, *52* (45), 11925–11929.
- (17) Lunkenbein, T.; Schumann, J.; Behrens, M.; Schlögl, R.; Willinger, M. G. Formation of a ZnO Overlayer in Industrial Cu/ZnO/Al<sub>2</sub>O<sub>3</sub> Catalysts Induced by Strong Metal-Support Interactions. *Angew. Chem., Int. Ed.* **2015**, *54* (15), 4544–4548.
- (18) Rodriguez, J. A.; Ma, S.; Liu, P.; Hrbek, J.; Evans, J.; Pérez, M. Activity of CeO<sub>x</sub> and TiO<sub>x</sub> Nanoparticles Grown on Au(111) in the Water-Gas Shift Reaction. *Science* **2007**, *318* (5857), 1757–1760.
- (19) Ma, Y.; Wang, J.; Goodman, K. R.; Head, A. R.; Tong, X.; Stacchiola, D. J.; White, M. G. Reactivity of a Zirconia-Copper Inverse Catalyst for CO<sub>2</sub> Hydrogenation. *J. Phys. Chem. C* **2020**, *124* (40), 22158–22172.
- (20) Rodriguez, J. A.; Hrbek, J. Inverse Oxide/Metal Catalysts: A Versatile Approach for Activity Tests and Mechanistic Studies. *Surf. Sci.* **2010**, *604* (3–4), 241–244.
- (21) Rodriguez, J. A.; Liu, P.; Graciani, J.; Senanayake, S. D.; Grinter, D. C.; Stacchiola, D.; Hrbek, J.; Fernández-Sanz, J. Inverse Oxide/Metal Catalysts in Fundamental Studies and Practical Applications: A Perspective of Recent Developments. *J. Phys. Chem. Lett.* **2016**, *7* (13), 2627–2639.
- (22) Palomino, R. M.; Gutiérrez, R. A.; Liu, Z.; Tenney, S.; Grinter, D. C.; Crumlin, E.; Waluyo, I.; Ramirez, P. J.; Rodriguez, J. A.; Senanayake, S. D. Inverse Catalysts for CO Oxidation: Enhanced Oxide-Metal Interactions in MgO/Au(111), CeO<sub>2</sub>/Au(111), and TiO<sub>2</sub>/Au(111). *ACS Sustain. Chem. Eng.* **2017**, *5* (11), 10783–10791.
- (23) Yang, F.; Graciani, J.; Evans, J.; Liu, P.; Hrbek, J.; Sanz, J. F.; Rodriguez, J. A. CO Oxidation on Inverse CeO<sub>x</sub>/Cu(111) Catalysts: High Catalytic Activity and Ceria-Promoted Dissociation of O<sub>2</sub>. *J. Am. Chem. Soc.* **2011**, *133* (10), 3444–3451.
- (24) Rodriguez, J. A.; Graciani, J.; Evans, J.; Park, J. B.; Yang, F.; Stacchiola, D.; Senanayake, S. D.; Ma, S.; Perez, M.; Liu, P.; Sanz, J. F.; Hrbek, J. Water-Gas Shift Reaction on a Highly Active Inverse CeO<sub>x</sub>/Cu(111) Catalyst: Unique Role of Ceria Nanoparticles. *Angew. Chem., Int. Ed.* **2009**, *48* (43), 8047–8050.
- (25) Lavroff, R. H.; Wang, J.; White, M. G.; Sautet, P.; Alexandrova, A. N. Mechanism of Stoichiometrically Governed Titanium Oxide Brownian Tree Formation on Stepped Au(111). *J. Phys. Chem. C* **2023**, *127* (17), 8030–8040.
- (26) Goodman, K. R.; Wang, J.; Ma, Y.; Tong, X.; Stacchiola, D. J.; White, M. G. Morphology and Reactivity of Size-Selected Titanium Oxide Nanoclusters on Au(111). *J. Chem. Phys.* **2020**, *152* (5), 054714 DOI: [10.1063/1.5134453](https://doi.org/10.1063/1.5134453).

- (27) Wang, J.; Ma, Y.; Mahapatra, M.; Kang, J.; Senanayake, S. D.; Tong, X.; Stacchiola, D. J.; White, M. G. Surface Structure of Mass-Selected Niobium Oxide Nanoclusters on Au(111). *Nanotechnology* **2021**, *32* (47), 475601.
- (28) Senanayake, S. D.; Stacchiola, D.; Rodriguez, J. A. Unique Properties of Ceria Nanoparticles Supported on Metals: Novel Inverse Ceria/Copper Catalysts for CO Oxidation and the Water-Gas Shift Reaction. *Acc. Chem. Res.* **2013**, *46* (8), 1702–1711.
- (29) Graciani, J.; Mudiyansele, K.; Xu, F.; Baber, A. E.; Evans, J.; Senanayake, S. D.; Stacchiola, D. J.; Liu, P.; Hrbek, J.; Fernández Sanz, J.; Rodriguez, J. A. Highly Active Copper-Ceria and Copper-Ceria-Titania Catalysts for Methanol Synthesis from CO<sub>2</sub>. *Science* **2014**, *345* (6196), 546–550.
- (30) Senanayake, S. D.; Ramirez, P. J.; Waluyo, I.; Kundu, S.; Mudiyansele, K.; Liu, Z.; Liu, Z.; Axnanda, S.; Stacchiola, D. J.; Evans, J.; Rodriguez, J. A. Hydrogenation of CO<sub>2</sub> to Methanol on CeOx/Cu(111) and ZnO/Cu(111) Catalysts: Role of the Metal-Oxide Interface and Importance of Ce<sup>3+</sup> Sites. *J. Phys. Chem. C* **2016**, *120* (3), 1778–1784.
- (31) Nakamura, J.; Nakamura, I.; Uchijima, T.; Watanabe, T.; Fujitani, T. Model Studies of Methanol Synthesis on Copper Catalysts. *Stud. Surf. Sci. Catal.* **1996**, *101*, 1389–1399.
- (32) Nakamura, J.; Choi, Y.; Fujitani, T. On the Issue of the Active Site and the Role of ZnO in Cu/ZnO Methanol Synthesis Catalysts. *Top. Catal.* **2003**, *22* (3–4), 277–285.
- (33) Kuld, S.; Thorhauge, M.; Falsig, H.; Elkjær, C. F.; Helveg, S.; Chorkendorff, I.; Sehested, J. Quantifying the Promotion of Cu Catalysts by ZnO for Methanol Synthesis. *Science* **2016**, *352* (6288), 969–974.
- (34) Reichenbach, T.; Walter, M.; Moseler, M.; Hammer, B.; Bruix, A. Effects of Gas-Phase Conditions and Particle Size on the Properties of Cu(111)-Supported ZnO Particles Revealed by Global Optimization and Ab Initio Thermodynamics. *J. Phys. Chem. C* **2019**, *123* (51), 30903–30916.
- (35) Yang, Y.; Evans, J.; Rodriguez, J. A.; White, M. G.; Liu, P. Fundamental Studies of Methanol Synthesis from CO<sub>2</sub> Hydrogenation on Cu(111), Cu Clusters, and Cu/ZnO(0001). *Phys. Chem. Chem. Phys.* **2010**, *12* (33), 9909–9917.
- (36) Huang, E.; Orozco, I.; Ramirez, P. J.; Liu, Z.; Zhang, F.; Mahapatra, M.; Nemšák, S.; Senanayake, S. D.; Rodriguez, J. A.; Liu, P. Selective Methane Oxidation to Methanol on ZnO/Cu<sub>2</sub>O/Cu(111) Catalysts: Multiple Site-Dependent Behaviors. *J. Am. Chem. Soc.* **2021**, *143* (45), 19018–19032.
- (37) Mahapatra, M.; Kang, J.; Ramirez, P. J.; Hamlyn, R.; Rui, N.; Liu, Z.; Orozco, I.; Senanayake, S. D.; Rodriguez, J. A. Growth, Structure, and Catalytic Properties of ZnOx Grown on CuO x/Cu(111) Surfaces. *J. Phys. Chem. C* **2018**, *122* (46), 26554–26562.
- (38) Amann, P.; Klötzer, B.; Degerman, D.; Köpfle, N.; Götsch, T.; Lömker, P.; Rameshan, C.; Ploner, K.; Bikaljevic, D.; Wang, H. Y.; Soldemo, M.; Shipilin, M.; Goodwin, C. M.; Gladh, J.; Halldin Stenlid, J.; Börner, M.; Schlueter, C.; Nilsson, A. The State of Zinc in Methanol Synthesis over a Zn/ZnO/Cu(211) Model Catalyst. *Science* **2022**, *376* (6593), 603–608.
- (39) Orozco, I.; Huang, E.; Gutiérrez, R. A.; Liu, Z.; Zhang, F.; Mahapatra, M.; Kang, J.; Kersell, H.; Nemsak, S.; Ramirez, P. J.; Senanayake, S. D.; Liu, P.; Rodriguez, J. A. Hydroxylation of ZnO/Cu(1 1 1) Inverse Catalysts under Ambient Water Vapor and the Water-Gas Shift Reaction. *J. Phys. D: Appl. Phys.* **2019**, *52* (45), 454001.
- (40) Liu, B. H.; Groot, I. M. N.; Pan, Q.; Shaikhutdinov, S.; Freund, H. J. Ultrathin Zn and ZnO Films on Cu(111) as Model Catalysts. *Appl. Catal. A Gen.* **2017**, *548*, 16–23.
- (41) Martin, O.; Mondelli, C.; Cervellino, A.; Ferri, D.; Curulla-Ferré, D.; Pérez-Ramírez, J. Operando Synchrotron X-Ray Powder Diffraction and Modulated-Excitation Infrared Spectroscopy Elucidate the CO<sub>2</sub> Promotion on a Commercial Methanol Synthesis Catalyst. *Angew. Chem., Int. Ed.* **2016**, *55* (37), 11031–11036.
- (42) Hansen, P. L.; Wagner, J. B.; Helveg, S.; Rostrup-Nielsen, J. R.; Clausen, B. S.; Topsøe, H. Atom-Resolved Imaging of Dynamic Shape Changes in Supported Copper Nanocrystals. *Science* **2002**, *295* (5562), 2053–2055.
- (43) Bikaljevic, D.; Rameshan, R.; Köpfle, N.; Götsch, T.; Mühlegger, E.; Schlögl, R.; Penner, S.; Memmel, N.; Klötzer, B. Structural and Kinetic Aspects of CO Oxidation on ZnOx-Modified Cu Surfaces. *Appl. Catal. A Gen.* **2019**, *572*, 151–157.
- (44) Mehar, V.; Huang, E.; Shi, R.; Rui, N.; Rosales, R.; Waluyo, I.; Hunt, A.; Liu, P.; Rodriguez, J. A. Microscopic Investigation of H<sub>2</sub> Reduced CuOx/Cu(111) and ZnO/CuOx/Cu(111) Inverse Catalysts: STM, AP-XPS, and DFT Studies. *ACS Catal.* **2023**, *13* (14), 9857–9870.
- (45) Bieniek, B.; Hofmann, O. T.; Rinke, P. Influence of Hydrogen on the Structure and Stability of Ultra-Thin ZnO on Metal Substrates. *Appl. Phys. Lett.* **2015**, *106* (13), 131602 DOI: 10.1063/1.4917015.
- (46) Fujitani, T.; Nakamura, I.; Uchijima, T.; Nakamura, J. The Kinetics and Mechanism of Methanol Synthesis by Hydrogenation of CO<sub>2</sub> over a Zn-Deposited Cu(111) Surface. *Surf. Sci.* **1997**, *383* (2–3), 285–298.
- (47) Nakamura, J.; Nakamura, I.; Uchijima, T.; Kanai, Y.; Watanabe, T.; Saito, M.; Fujitani, T. A Surface Science Investigation of Methanol Synthesis over a Zn-Deposited Polycrystalline Cu Surface. *J. Catal.* **1996**, *160* (1), 65–75.
- (48) Palomino, R. M.; Ramirez, P. J.; Liu, Z.; Hamlyn, R.; Waluyo, I.; Mahapatra, M.; Orozco, I.; Hunt, A.; Simonovis, J. P.; Senanayake, S. D.; Rodriguez, J. A. Hydrogenation of CO<sub>2</sub> on ZnO/Cu(100) and ZnO/Cu(111) Catalysts: Role of Copper Structure and Metal-Oxide Interface in Methanol Synthesis. *J. Phys. Chem. B* **2018**, *122* (2), 794–800.
- (49) Klimeš, J.; Bowler, D. R.; Michaelides, A. Chemical Accuracy for the van Der Waals Density Functional. *J. Phys. Condens. Matter* **2010**, *22* (2), 022201.
- (50) Zhai, H.; Alexandrova, A. N. Fluxionality of Catalytic Clusters: When It Matters and How to Address It. *ACS Catal.* **2017**, *7* (3), 1905–1911.
- (51) Weirum, G.; Barcaro, G.; Fortunelli, A.; Weber, F.; Schennach, R.; Surnev, S.; Netzer, F. P. Growth and Surface Structure of Zinc Oxide Layers on a Pd(111) Surface. *J. Phys. Chem. C* **2010**, *114* (36), 15432–15439.
- (52) Sawant, K. J.; Zeng, Z.; Greeley, J. P. Universal Properties of Metal-Supported Oxide Films from Linear Scaling Relationships: Elucidation of Mechanistic Origins of Strong Metal-Support Interactions. *Chem. Sci.* **2023**, *14* (12), 3206–3214.
- (53) Li, D.; Xu, F.; Tang, X.; Dai, S.; Pu, T.; Liu, X.; Tian, P.; Xuan, F.; Xu, Z.; Wachs, I. E.; Zhu, M. Induced Activation of the Commercial Cu/ZnO/Al<sub>2</sub>O<sub>3</sub> Catalyst for the Steam Reforming of Methanol. *Nat. Catal.* **2022**, *5* (2), 99–108.
- (54) Kresse, G.; Furthmüller, J. Efficiency of Ab-Initio Total Energy Calculations for Metals and Semiconductors Using a Plane-Wave Basis Set. *Comput. Mater. Sci.* **1996**, *6* (1), 15–50.
- (55) Kresse, G.; Furthmüller, J. Efficient Iterative Schemes for Ab Initio Total-Energy Calculations Using a Plane-Wave Basis Set. *Phys. Rev. B* **1996**, *54* (16), 11169–11186.
- (56) Kresse, G.; Hafner, J. Ab Initio Molecular Dynamics for Liquid Metals. *Phys. Rev. B* **1993**, *47* (1), 558–561.
- (57) Perdew, J. P.; Burke, K.; Ernzerhof, M. Generalized Gradient Approximation Made Simple. *Phys. Rev. Lett.* **1996**, *77* (18), 3865–3868.
- (58) Vázquez-Parga, D.; Fernández-Martínez, A.; Viñes, F. Quantifying the Accuracy of Density Functionals on Transition Metal Bulk and Surface Properties. *J. Chem. Theory Comput.* **2023**, *19* (22), 8285–8292.
- (59) Blöchl, P. E. Projector Augmented-Wave Method. *Phys. Rev. B* **1994**, *50* (24), 17953–17979.
- (60) Grimme, S.; Antony, J.; Ehrlich, S.; Krieg, H. A Consistent and Accurate Ab Initio Parametrization of Density Functional Dispersion Correction (DFT-D) for the 94 Elements H-Pu. *J. Chem. Phys.* **2010**, *132* (15), 154104 DOI: 10.1063/1.3382344.

(61) Neugebauer, J.; Scheffler, M. Adsorbate-Substrate and Adsorbate-Adsorbate Interactions of Na and K Adlayers on Al(111). *Phys. Rev. B* **1992**, *46* (24), 16067–16080.

(62) Krukau, A. V.; Vydrov, O. A.; Izmaylov, A. F.; Scuseria, G. E. Influence of the Exchange Screening Parameter on the Performance of Screened Hybrid Functionals. *J. Chem. Phys.* **2006**, *125* (22), 224106 DOI: 10.1063/1.2404663.

(63) Hjorth Larsen, A.; Jørgen Mortensen, J.; Blomqvist, J.; Castelli, I. E.; Christensen, R.; Dulak, M.; Friis, J.; Groves, M. N.; Hammer, B.; Hargus, C.; Hermes, E. D.; Jennings, P. C.; Bjerre Jensen, P.; Kermode, J.; Kitchin, J. R.; Leonhard Kolsbjerg, E.; Kubal, J.; Kaasbjerg, K.; Lysgaard, S.; Bergmann Maronsson, J.; Maxson, T.; Olsen, T.; Pastewka, L.; Peterson, A.; Rostgaard, C.; Schiøtz, J.; Schütt, O.; Strange, M.; Thygesen, K. S.; Vegge, T.; Vilhelmsen, L.; Walter, M.; Zeng, Z.; Jacobsen, K. W. The Atomic Simulation Environment - A Python Library for Working with Atoms. *J. Phys. Cond. Matter.* **2017**, *29*, 273002.

(64) Bahn, S. R.; Jacobsen, K. W. An Object-Oriented Scripting Interface to a Legacy Electronic Structure Code. *Comput. Sci. Eng.* **2002**, *4* (3), 56–66.

(65) Zhang, Z.; Wei, Z.; Sautet, P.; Alexandrova, A. N. Hydrogen-Induced Restructuring of a Cu(100) Electrode in Electroreduction Conditions. *J. Am. Chem. Soc.* **2022**, *144* (42), 19284–19293.

(66) Stukowski, A. Visualization and Analysis of Atomistic Simulation Data with OVITO-the Open Visualization Tool. *Modell. Simul. Mater. Sci. Eng.* **2010**, *18* (1), 015012.